JOURNAL OF SOLID STATE CHEMISTRY 9, 345–351 (1974)

Crystal Chemistry in the System $MSbO_3$*

H. Y-P. HONG, J. A. KAFALAS AND J. B. GOODENOUGH

Lincoln Laboratory, Massachusetts Institute of Technology, Lexington, Massachusetts 02173

Received July 5, 1973

Cubic, disordered phases of the compounds $MSbO_3$ (M = Li, Na, K, Rb, Tl, and Ag) have been investigated. $KSbO_3$ is readily synthesized in the disordered, cubic structure at high pressure, and the other isomorphic compounds were obtained by ion exchange. The structures of $NaSbO_3$ and $AgSbO_3$, which have space group *Im*3, were solved by X-ray single-crystal analysis. The structures contain an essentially rigid SbO_3 subarray consisting of pairs of edge-shared octahedra sharing common corners. Within this subarray, face-shared octahedra form ⟨111⟩ tunnels that intersect at the origin and body center of the unit cell, and the M^+ ions are randomly distributed over two positions within these tunnels. Ordered, cubic phases have the primitive-cubic space group *Pn*3. The two M positions are different for Na^+ and for Ag^+ ions. At one of the Ag^+-ion positions, the Ag–O bond length is only 2.26 Å, consistent with the gray-black color of $AgSbO_3$. Deformation of the $4d^{10}$ Ag^+-ion core by $4d$–$5s$ hybridization appears to be induced by Ag–O covalent bonding. This conclusion is compatible with the observation that ion exchange is reversible for all compounds but $AgSbO_3$. Several properties of these compounds are compared with the super ionic conductors $M_2O{\cdot}11Al_2O_3$ β-alumina.

I. Introduction

Unlike the M^+NbO_3 and M^+TaO_3 compounds, the M^+SbO_3 compounds do not form structures having 180° Sb–O–Sb linkages, presumably because this is inhibited by covalency (*1*). Thus $KSbO_3$ does not form the cubic perovskite structure. At atmospheric pressure it generally has the rhombohedral ilmenite structure. However, Spiegelberg (*2*) reported synthesizing two cubic phases of $KSbO_3$ by annealing for 3 wk at 1000°C. One of these was primitive, with space group *Pn*3. The other was body-centered, but Spiegelberg was unable to determine its space group.

In the primitive-cubic $KSbO_3$, pairs of SbO_6 octahedra share common edges to form Sb_2O_{10} clusters (*2*). These clusters share corners to form the network shown in Fig. 1. The network contains empty tunnels of face-shared octahedra that run parallel to the ⟨111⟩ directions and intersect at the center of the front face in Fig. 1. This origin is itself a large octahedral interstice, and along any ⟨111⟩ direction there are three additional octahedral positions between the origin and its body-center equivalent. Each of the shared faces along the tunnels consists of either O_1 or O_2

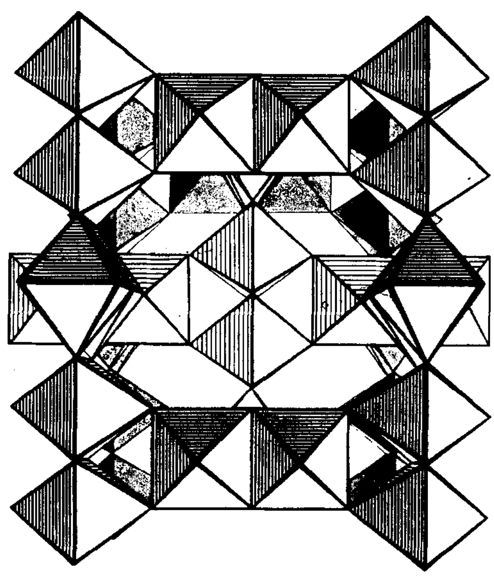

FIG. 1. The cubic SbO_3 matrix found by Spiegelberg (*2*) for cubic $KSbO_3$ having the space group *Pn*3 and ordered K^+-ion positions.

* This work was sponsored by the Department of the Air Force.

oxygen atoms. The order of the faces is O_1–O_2–O_2–O_1, and the triangular area of an O_1 face is somewhat larger than that of an O_2 face. The primitive unit cell contains $K_{12}Sb_{12}O_{36}$, and the K^+ ions are ordered within the octahedral sites of these tunnels: eight in O_1–O_2 octahedra along four tetrahedral directions from the origin, and four in O_2–O_2 octahedra along the remaining four directions.

The body-centered cell is closely related to the primitive unit cell. A body-centered-cubic *I*23 phase containing a network similar to the one in Fig. 1 has been reported (*3*) for $La_4ORe_6O_{18}$. In this structure an oxygen is located at the origin and four La^{3+} ions occupy O_1–O_2 octahedra in $[1,1,1]$, $[\bar{1},\bar{1},1]$, $[\bar{1},1,\bar{1}]$, $[1,\bar{1},\bar{1}]$ directions. It is therefore reasonable to assume that the body-centered form of $KSbO_3$ contains the SbO_3 network of Fig. 1 with the K^+ ions disordered over the octahedral sites of the tunnels. This assignment gives space group *Im*3.

The possibility of alkali-ion exchange was suggested by the cubic $KSbO_3$ structures. The tunnels of face-shared octahedra running parallel to the $\langle 111 \rangle$ directions are not completely occupied, so high alkali-ion conductivity may be anticipated, provided the M^+ ion is small enough to move through the O_2 faces. Since the O_2–O_2 and O_1–O_1 octahedra are flattened, making relatively open O_1 and O_2 faces, the structure also suggests that the alkali-ion conductivity may be comparable to that of sodium β-alumina, $Na_2O \cdot 11Al_2O_3$. Therefore, in addition to the structure refinements for several $MSbO_3$ compounds, we compare their properties with those of β-alumina.

II. Preparation

The cubic forms of $KSbO_3$ were prepared from the ilmenite form in a high-pressure "belt" apparatus (*4*) capable of developing 90 kbar and equipped with an internal graphite heater. The ilmenite phase was subjected to pressures in excess of 20 kbar and then to a temperature of 700°C for 30 min. The specimen was subsequently quenched to room temperature before the pressure was released. This treatment normally yielded the disordered, body-centered form *Im*3 of cubic $KSbO_3$. Subsequent heat treatment (1200°C for 16 hr) of this form at atmospheric pressure yielded the ordered *Pn*3 form.

$RbSbO_3$ and $TlSbO_3$ were prepared from the products of stoichiometric amounts of Rb_2CO_3 or Tl_2CO_3 and Sb_2O_3 air-fired at 900°C. The products were encapsulated in gold foil and subjected to the desired pressure in the belt apparatus. The temperature was raised to 900°C for 30 min and quenched before the pressure was released. At 20 kbar, $RbSbO_3$ was obtained in the ordered *Pn*3 form. Considerably higher pressure gave the disordered *Im*3 form. Pressures in excess of 20 kbar yielded a cubic $TlSbO_3$ phase having a doubled cell edge. Oscillation and Weissenberg pictures of a single crystal showed a face-centered-cubic cell with diffraction symmetry *m*3, which indicates space group *F*23 or *Fm*3.

Attempts to prepare $NaSbO_3$, $AgSbO_3$ and $LiSbO_3$ by the same high-pressure technique gave, respectively, an ilmenite, a pyrochlore, and an orthorhombic phase. However, we have been able to prepare each of these compounds in the body-centered *Im*3 phase by an ion-exchange method. A cubic $KSbO_3$ phase was mixed with molten MNO_3 (M = Li, Na, Rb, Tl, or Ag) in about 1:10 molar ratios for a few hours. In each case, the K^+ ions appeared to be completely replaced by the M^+ ions, since the X-ray powder pattern showed significant changes in the cell parameters (see Table IV) and the final cell parameter was independent of the initial compound: $KSbO_3$ or $TlSbO_3$, for example. Except for $AgSbO_3$, the process is reversible. If one of the other $MSbO_3$ phases is mixed with molten KNO_3, for example, the *Im*3 $KSbO_3$ phase is recovered and has the initial cell size.

Structure determinations of $NaSbO_3$ and $AgSbO_3$ were made on single crystals prepared from single crystals of $TlSbO_3$ by ion exchange in molten $NaNO_3$ and $AgNO_3$, respectively. The single crystals of $TlSbO_3$ were selected from the powder product of a high-pressure reaction (20 kbar at 700°C for 30 min) of the product of an 800°C reaction of Tl_2CO_3 and Sb_2O_3.

III. Structure

Weissenberg photographs of single crystals of $NaSbO_3$ and $AgSbO_3$, prepared from $TlSbO_3$ by ion exchange, showed they were cubic, but with the low symmetry *m*3. Systematic absences were observed for $h + k + l = 2n + 1$, consistent with space groups *I*23, $I2_13$ and *Im*3.

X-Ray intensity measurements of three-dimensional data were taken to $2\theta = 60°$ with a GE XRD-5 diffractometer using Zr-filtered Mo$K\alpha$ radiation at a 5° takeoff angle. Each peak height was counted for 10 sec, and backgrounds were counted for 10 sec at $\pm 2^\circ$ in 2θ off the peak. The Lorentz, polarization and ϕ-angle absorption corrections were applied. Both crystals were about 0.2 mm cube, and three-dimensional absorption corrections were considered not necessary.

A three-dimensional Patterson map was calculated and interpreted on the basis of space group *Im*3. As anticipated from the strong similarity between the powder patterns of primitive and body-centered $KSbO_3$ as well as from the ease of ion exchange, the SbO_3 network appears to be similar to Fig. 1, which was identified for the primitive-cubic $KSbO_3$ structure. Therefore, the Sb^{5+}-ion and O^{2-}-ion positions obtained by Spiegelberg (*2*) for the *Pn*3 form of $KSbO_3$ were used for the initial refinement based on *Im*3. The least-squares program gave a reliability factor $R = 0.17$ for $NaSbO_3$ and $R = 0.18$ for $AgSbO_3$. From the calculated structure factors based on this model, a Fourier map for $NaSbO_3$ revealed two Na^+-ion positions at (x,x,x): a larger electron density near $x = \frac{1}{8}$ and a lower electron density at $x = \frac{1}{4}$. There was zero electron density at (0,0,0), the center of the front face in Fig. 1. The Fourier map for $AgSbO_3$ also gave two Ag^+-ion positions at (x,x,x): a smaller electron density for x approaching $\frac{1}{8}$ and a stronger about midway in the interval $\frac{1}{8} < x < \frac{1}{4}$. With these atomic positions and anisotropic temperature factors, a few refinement cycles reduced the reliability factors to $R = 0.07$ for $NaSbO_3$ for all 238 reflections and $R = 0.08$ for $AgSbO_3$ for all 138 reflections. Refinements based on the space groups *I*23 and $I2_13$ both gave higher R factors and unrealistic temperature factors. Therefore, the space group *Im*3 was confirmed. The scattering factors used for K, Sb^{5+}, O are those published (*5*) with anomalous dispersion coefficients for Mo radiation (*6*). The final atomic positions, occupancy factors and anisotropic temperature factors are shown in Table I for $NaSbO_3$, in Table II for $AgSbO_3$. The bond distances for both compounds are shown in Table III.

It is instructive to locate the positions of the M^+ ions relative to the O_1 and O_2 faces along a $\langle 111 \rangle$-axis tunnel. In $NaSbO_3$, the normalized distance from an O_1^{2-} ion at (0.356, 0, 0) to a Na^+ ion at (x,x,x) is

$$D_1/a = [(x - 0.356)^2 + x^2 + x^2]^{1/2} = (3x^2 - 0.712x + 0.1267)^{1/2}, \quad (1)$$

which gives a minimum separation ($a = 9.3775$ Å, Table IV)

$$D_{1,\min} = 2.726 \text{ Å at } x = 0.1187, \quad (2)$$

the center of an O_1 face. Similarly, the normalized distance from an O^{2-} ion at (0, 0.334, 0.287) is

$$D_2/a = [x^2 + (x - 0.334)^2 + (x - 0.287)^2]^{1/2} = (3x^2 - 1.242x + 0.1939)^{1/2}, \quad (3)$$

which has a minimum value

$$D_{2,\min} = 2.40 \text{ Å at } x = 0.207, \quad (4)$$

the center of an O_2 face. Since the ionic Na–O distance is 2.42 Å, it is apparent that the Na^+ ions should move along the tunnels with a relatively small activation energy. Moreover, from Table I, the Na_1 position is located at $x = 0.123$, which places it near the center of an O_1–O_2 octahedron.

TABLE I

ATOMIC POSITIONS AND THERMAL PARAMETERS OF $NaSbO_3$

Atom:	Sb	O_1	O_2	Na_1	Na_2
Position:	12(*e*)	12(*d*)	24(*g*)	16(*f*)	8(*c*)
Occupancy factor:				0.82(2)	0.29(3)
x	0.8384(2)	0.356(2)	0	0.1229(9)	$\frac{1}{4}$
y	0	0	0.334(1)	0.1229(9)	$\frac{1}{4}$
z	$\frac{1}{2}$	0	0.287(1)	0.1229(9)	$\frac{1}{4}$
β_{11}	0.0014(2)	0.006(3)	0.000(1)	0.006(1)	0.005(1)
β_{22}	0.0016(2)	0.000(2)	0.000(1)	0.006(1)	0.005(1)
β_{33}	0.0018(2)	0.006(2)	0.005(2)	0.006(1)	0.005(1)
β_{12}	0	0	0	0.003(1)	0
β_{13}	0	0	0	0.003(1)	0
β_{23}	0	0	0.000(1)	0.003(1)	0

TABLE II

ATOMIC POSITIONS AND THERMAL PARAMETERS OF $AgSbO_3$

Atom:	Sb	O_1	O_2	Ag_1	Ag_2
Position:	12(*e*)	12(*d*)	24(*g*)	16(*f*)	16(*f*)
Occupancy factor:				0.33(3)	0.44(2)
x	0.8393(4)	0.371(4)	0	0.111(1)	0.184(1)
y	0	0	0.296(7)	0.111(1)	0.184(1)
z	$\frac{1}{2}$	0	0.291(4)	0.111(1)	0.184(1)
β_{11}	0.0007(4)	0.002(4)	0.009(5)	0.013(2)	0.012(1)
β_{22}	0.0025(5)	0.006(5)	0.05(1)	0.013(2)	0.012(1)
β_{33}	0.0028(5)	0.002(4)	0.008(5)	0.013(2)	0.012(1)
β_{12}	0	0	0	0	0.006(1)
β_{13}	0	0	0	0	0.006(1)
β_{23}	0	0	0.012(9)	0	0.006(1)

TABLE III

BOND DISTANCES (Å) OF $NaSbO_3$ AND $AgSbO_3$

	$NaSbO_3$	$AgSbO_3$
Octahedron around Sb^{5+}		
$Sb–O_1$ 2 ×	2.027	1.936
$Sb–O_2$ 2 ×	1.949	2.279
2 ×	1.996	2.006
Nearest O^{2-} neighbors		
$O_1–O_1$ 1 ×	2.692	2.421
$O_1–O_2$ 4 ×	2.864	3.002
$O_1–O_2$ 2 ×	3.202	2.881
$O_1–O_2$ 2 ×	2.701	2.828
$O_2–O_2$ 4 ×	2.774	2.866
Neighbors of Na^+	Neighbors of Ag^+	
$Na_1–O_1$ 3 × 2.730	$Ag_1–O_1$ 3 × 2.858	
$Na_1–O_2$ 3 × 2.760	$Ag_1–O_2$ 3 × 2.644	
$Na_2–O_2$ 6 × 2.650	$Ag_2–O_1$ 3 × 3.014	
$Na_1–Na_1$ 3 × 2.303	$Ag_2–O_2$ 3 × 2.260	
$Na_1–Na_1$ 3 × 3.257	$Ag_1–Ag_2$ 3 × 2.935	
$Na_1–Na_2$ 2 × 2.094	$O_1–O_1$ 4.950 (triangle)	
$O_1–O_1$ 4.761 (triangle)	$O_2–O_2$ 3.910 (triangle)	
$O_2–O_2$ 4.447 (triangle)		

It is displaced from the position $x = 0.127$, where $D_1 = D_2$, toward the origin—presumably because of electrostatic interactions between Na^+ ions at neighboring Na_I positions within the tunnels—to give three $Na_1–O_1$ distances of 2.73 Å and three $Na_1–O_2$ distances of 2.76 Å. From the relative intensities of the electron densities at positions Na_I and Na_2, it appears that a Na^+ ion at a Na_2 position inhibits occupancy of the near-neighbor $O_1–O_2$ sites on opposite sides of it. Moreover, any electrostatic forces between Na^+ ions produce a zero mean Na_2 displacement, and

TABLE IV

LATTICE CONSTANTS OF $MSbO_3$ POLYMORPHS WITH SPACE GROUP *Im*3

Compound	*a* (Å)
$AgSbO_3$[a]	9.404(3)
$LiSbO_3$	9.465(8)
$NaSbO_3$[a]	9.378(3)
$KSbO_3$	9.563(8)
$RbSbO_3$	9.698(8)
$TlSbO_3$	19.30(1)

[a] Were obtained from GE XRD single-crystal diffractometer, the rest were obtained from powder diffractometer.

all Na_2–O_2 distances are 2.65 Å. Figure 2a gives a schematic representation of the random Na^+-ion distribution.

In $AgSbO_3$, on the other hand, the Ag^+ ions

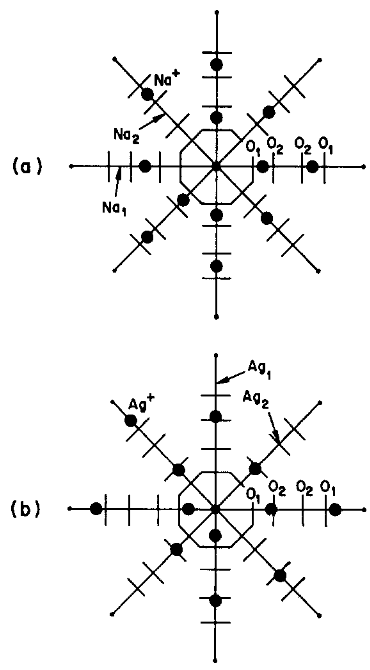

FIG. 2. Schematic representation of the eight ⟨111⟩ channels branching from the origin to the neighboring body-center positions: (a) $NaSbO_3$ and (b) $AgSbO_3$. The O_1 and O_2 octahedral-site faces perpendicular to the channels are represented by straight lines. Possible distributions of M^+ ions over the M_1 and M_2 positions are also indicated.

are not located at or near the centers of the O_2–O_2 or O_1–O_2 octahedra. Since

$$D_1/a = (3x^2 - 0.742x + 0.1376)^{1/2}, \quad (5)$$

$$D_2/a = (3x^2 - 1.176x + 0.1729)^{1/2}, \quad (6)$$

and $a = 9.4038$ Å, it follows that

$$D_{1,\,\mathrm{min}} = 2.849 \text{ Å at } x = 0.124, \quad (7)$$

$$D_{2,\,\mathrm{min}} = 2.258 \text{ Å at } x = 0.196. \quad (8)$$

Therefore, the Ag_2 position at $x = 0.184$ is located close to an O_2 face and forms an unusually short Ag–O bond of only 2.260 Å. It would appear that this strong bond traps the Ag^+ ion, hindering its transfer to the O_2–O_2 octahedral site at $x = 0.25$. At least such an explanation would account for the zero electron density at $x = 0.25$ and the inability to exchange Ag^+ ions reversibly.

In $AgSbO_3$, the SbO_3 matrix is deformed so as to give much smaller O_2–O_2 than O_1–O_1 separations, as can be seen from Eqs. (7) and (8). In fact, $D_1 = D_2$ at $x = 0.081$, which is well inside the large octahedral sites of all O_1 ions. The Ag_1 positions at $x = 0.111$ are also inside, as can be seen from Eq. (7). Since the Ag_2–O_2 distances are strikingly shorter than the Ag_1–O_2 distances, the Ag^+ ions should occupy preferentially the Ag_2 positions. However, the Ag_2–Ag_2 separation across a common O_2–O_2 site is so short that electrostatic Ag^+–Ag^+ interactions can be expected to inhibit occupancy of both positions. Therefore, the 12 Ag^+ ions per unit cell can be distributed preferentially among only 8 of the 16 Ag_2 positions. For an infinite Ag_2-site preference energy, the electron-density ratio for the two sites would be $Ag_1/Ag_2 = \frac{1}{2}$. From Table II, a ratio $Ag_1/Ag_2 = \frac{3}{4}$ is observed, indicating a finite Ag_2-site preference energy. This leads to the random Ag^+-ion distribution shown schematically in Fig. 2b. An Ag_1 position at $x = 0.111$ suggests that Ag^+–Ag^+ pair interactions within a tunnel have been strong enough to displace one Ag^+ ion from an Ag_2 to an Ag_1 position, but that the interactions between ions at Ag_1 positions have kept $x > 0.081$, the position where $D_1 = D_2$.

The Ag^+ ions at Ag_1 positions appear to be ionically bound, those at Ag_2 positions to be covalently bound to three O_2 ions. Such a variation in Ag–O bonding is characteristic of Ag^+-ion salts. Where the oxygens have orbitals available for strong coordinate covalence, there a $4d$–$5s$ hybridization may be induced on the Ag^+ ions. Such hybridization changes the shape of the $4d^{10}$ core from a sphere to an ellipsoid, thereby allowing stronger Ag–O bonding along the shorter axis, or axes, of the ellipsoid by reducing the extension of the core–core repulsive forces. In black Ag_2O, linear O–Ag–O bonding produces Ag–O bond lengths of only 2.05 Å. Each O^{2-} ion has four near-neighbor Ag^+ ions in tetrahedral coordination, and sp^3 hybridization at the oxygen is coupled to sd_σ hybridization at the silver to allow strongly covalent bonding. In white $AgClO_3$, on the other hand, the oxygen atoms use all their $2s2p$ orbitals to bond preferentially with the chlorine atoms, so no $4d$–$5s$ hybridization is induced on the Ag^+ ions and the Ag–O separations vary from 2.47 to 2.55 Å. Ag–O bond lengths of intermediate size are common. Yellow Ag_2CO_3, for example, has an Ag–O separation of 2.30 Å. Interestingly, the color of the silver salts may be well correlated with the Ag–O separation R. For $R > 2.4$ Å, the compounds are white, and for $R < 2.25$ Å the compounds are black. $AgSbO_3$, which contains an $R = 2.25$ Å, is gray-black. Compounds having $R = 2.30$–2.34 are yellow or red.

Interpretation of the color changes with bond length proceeds as follows. White compounds have a large ($\gtrsim 2.8$ eV) energy gap E_g between the valence and conduction bands. Black compounds have an $E_g \lesssim 1.7$ eV. Therefore, the color changes indicate a band gap that decreases with increasing strength of the bond. This variation is just opposite to that experienced in covalent elements crystallizing in the diamond structure. In general, stronger bonding (shorter bond lengths) increases the gap between the mean energies of the occupied bonding orbitals and the empty antibonding orbitals. Therefore, it is difficult to understand the color changes in the silver salts unless the top of the valence band is composed of nonbonding core orbitals—the $4d$ or hybridized ($4d$–$5s$) orbitals at the Ag^+ ions—rather than the bonding $O^{2-}:2p$ orbitals. Since hybridization raises the $4d$ levels relative to the $5s$ levels, it should decrease the energy gap between the top of the $4d$-like bands and the bottom of the $5s$-like bands, as illustrated schematically in Fig. 3. Therefore, if the top of the valence band is primarily $4d$-like and reduction of the Ag–O bond length requires greater $5s$ hybridization, the energy gap E_g will decrease with decreasing Ag–O bond length, as observed. Furthermore, a relatively small energy separation between $4d$ core orbitals and $5s$ orbitals is required for appreciable deformation of the core via hybridization. Silver appears to be particularly susceptible to such a deformation of its core.

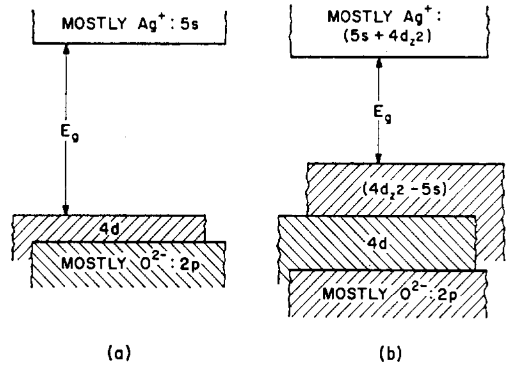

FIG. 3. Schematic energy diagrams for Ag^+ oxides: (a) long Ag–O bonds, (b) short Ag–O bonds (Ag_2O).

In $AgSbO_3$, each oxygen forms two strongly covalent Sb–O bonds. The Sb–O_I–Sb angle is only a little larger than 90°, and the remaining p_π orbital perpendicular to the plane of that angle does not extend into the M^+-ion tunnels. Therefore, ionic Ag–O_1 bond lengths are to be expected. The Sb–O_2–Sb angle, on the other hand, is somewhat larger than 120°, indicating strong hybridization of sp^3 orbitals at the O_2 position. Moreover, the two remaining hybrid orbitals are directed into the tunnels where they can induce covalent Ag–O bonding. Therefore, the short Ag_2–O_2 bonds are to be anticipated.

Several $MSbO_3$ compounds having the cubic $Im3$ structure have been prepared from $KSbO_3$ by ion exchange. Table IV shows the lattice constants, obtained from both powder and single-crystal X-ray data, for the various polymorphs having space group $Im3$. With the exception of $LiSbO_3$, the lattice constants scale with the M^+-ion radii. The highly ionic, large ions K^+, Tl^+ and Rb^+ can be expected to occupy the O_1–O_2 and O_2–O_2 sites, as does the Na^+ ion, whereas the small Li^+ ion may tend to occupy a position in or near an O_2 face, as does the Ag^+ ion. The presence of ionic Li^+ ions in octahedral-site faces would expand the cubic lattice parameter relative to the value extrapolated from $RbSbO_3$, $KSbO_3$ and $NaSbO_3$. That a similar expansion is not found in $AgSbO_3$ is attributed to the core deformation resulting from Ag–O covalent bonding, which induces $4d$–$5s$ hybridization at the Ag^+ ions.

IV. Comparisons with β-Alumina

Of the 26 octahedral tunnel sites per primitive unit cell, only 12 are occupied by M^+ ions. Therefore, excellent three-dimensional conductivity can be anticipated. Our data provide the following comparisons between the $MSbO_3$ compounds and the so-called super ionic conductor β-alumina:

1. In both, the M^+ ions can be ion-exchanged in molten salts and the exchanges are reversible, except for $AgSbO_3$ which can be only partially exchanged. In silver β-alumina (*7*), the shortest Ag–O distance is 2.424 Å, which is large enough to be primarily ionic, whereas in $AgSbO_3$ the shortest Ag–O distance 2.260 Å is small enough to be primarily covalent. Moreover, the reduced band gap introduced by this covalence enhances the probability of doping the crystal, thereby introducing electronic as well as ionic charge carriers.

2. Both $LiSbO_3$ and $Li_2O \cdot 11Al_2O_3$ have lattice parameters anomalously larger than predicted from extrapolation of the parameters for the other M^+ ions.

3. In both, M^+ ions only partially occupy the available M positions. Sodium β-alumina contains four Na_1–O_2 distances greater than 2.71 Å (*8*), whereas $NaSbO_3$ has six Na_2–O_2 distances at 2.65 Å. These distances are all larger than the sum of the ionic radii. Moreover, in $Na_2O \cdot 11Al_2O_3$ the Na^+ ions must pass through a common octahedral-site edge, whereas in $NaSbO_3$ they pass through octahedral-site faces. Therefore, we may anticipate comparable ionic mobilities in the two structures.

4. In β-alumina, the M^+ ions are constrained to two-dimensional motion, whereas in $MSbO_3$ they may move in three dimensions, the ⟨111⟩ tunnels intersecting at common octahedral sites at the origin. Thus the Na^+-ion transport mechanism is similar to the Ag^+-ion diffusion in $RbAg_4I_5$, where the Ag^+ ions partially occupy a three-dimensional network of tetrahedra sharing common faces (*9*). Similar diffusion paths exist in other silver halides and chalcogenides (*10–14*).

5. Surprisingly, structure refinements of sodium β-alumina indicate about 29% excess sodium (*7*). Similarly, our intensity data indicate an excess sodium concentration of 28.7% in nominal $NaSbO_3$. Nevertheless, electrical neutrality is maintained in both compounds. The location and charge-neutrality mechanism of the excess sodium has not been identified in either compound.

6. Preliminary ac measurements indicate that the ionic conductivity of $NaSbO_3$ compares favorably with that found for $Na_2O \cdot 11Al_2O_3$.

7. It is difficult to prepare dense ceramic specimens of β-alumina that do not develop leaks. It is also difficult to prepare dense ceramics of metastable $NaSbO_3$, since not pressing is confined to the temperature interval $T < 500°C$. A more fundamental difficulty is that ceramic $NaSbO_3$ is slowly attacked by molten sodium. Nevertheless, the transport data demonstrate that "skeleton" structures of the *Im*3 type (here the SbO_3 matrix forms the skeleton) promise to be important for fast-ion transport.

Acknowledgment

We thank C. H. Anderson, Jr. and D. M. Tracy for technical assistance.

References

1. J. B. Goodenough and J. A. Kafalas, *J. Solid State Chem.*, in press.
2. P. Spiegelberg, *Ark. Kemi* **14A**, 1 (1940).
3. J. M. Longo and A. W. Sleight, *Inorg. Chem.* **7**, 108 (1968).
4. H. T. Hall, *Rev. Sci. Inst.* **31**, 125 (1960).
5. D. T. Cromer and J. T. Waber, *Acta Crystallogr.* **18**, 104 (1965).
6. D. T. Cromer, *Acta Crystallogr.* **18**, 17 (1965).
7. C. R. Peters, M. Bettman, J. W. Moore, and M. D. Glick, *Acta Crystallogr. Sect. B* **27**, 1826 (1971).
8. W. L. Roth, *J. Solid State Chem.* **4**, 60 (1972).
9. S. Geller, *Science* **157**, 310 (1967).
10. L. W. Strock, *Z. Phys. Chem. Abt. B* **25**, 441 (1934).
11. L. W. Strock, *Z. Phys. Chem., Abt. B* **31**, 132 (1936).
12. P. Rahlfs, *Z. Phys. Chem., Abt. B* **31**, 157 (1936).
13. S. Hoshino, *J. Phys. Soc. Jap.* **7**, 560 (1952).
14. B. Reuter and K. Hardel, *Z. Anorg. Allg. Chem.* **340**, 168 (1965).